arXiv:1611.08689v1 [cond-mat.mtrl-sci] 26 Nov 2016

# Band alignment and charge transfer in complex oxide interfaces

Zhicheng Zhong[1] and Philipp Hansmann[1]

[1] *Max-Planck-Institut für Festkörperforschung, Heisenbergstrasse 1, 70569 Stuttgart, Germany*

(Dated: November 29, 2016)

The synthesis of transition metal heterostructures is currently one of the most vivid fields in the design of novel functional materials. In this paper we propose a simple scheme to predict *band alignment* and *charge transfer* in complex oxide interfaces. For semiconductor heterostructures band alignment rules like the well known Anderson or Schottky-Mott rule are based on comparison of the work function or electron affinity of the bulk components. This scheme breaks down for oxides due to the invalidity of a single workfunction approximation as recently shown (Phys. Rev. B 93, 235116; Adv. Funct. Mater. 26, 5471). Here we propose a new scheme which is built on a continuity condition of valence states originating in the compounds' shared network of oxygen. It allows for the prediction of sign and relative amplitude of the intrinsic charge transfer, taking as input only information about the bulk properties of the components. We support our claims by numerical density functional theory simulations as well as (where available) experimental evidence. Specific applications include i) controlled doping of $SrTiO_3$ layers with the use of $4d$ and $5d$ transition metal oxides and ii) the control of magnetic ordering in manganites through tuned charge transfer.

PACS numbers: 73.20.-r, 73.21.-b,79.60.Jv

## I. INTRODUCTION

Until today semiconductors present the most important class of functional materials for electronic applications. Their usage in electronic components and the continuous development of new devices keeps on pushing the limits of technology. In almost all such devices the key functionality originates not in the physics of the bulk, but in the peculiarities of interfaces [1]. Yet, semiconductor devices have intrinsic limitations: i) the characteristic length scales are relatively large so that further downscaling (current state of the art is $7nm$ technology) becomes very unlikely and Moore's law is bound to end; ii) solely charge degrees of freedom are exploited. Transition metal oxides (TMO) on the other hand provide spin, orbital, charge and lattice degrees of freedom [2, 3] and are therefore viewed as one of the best candidates to replace semiconductors in future electronic device. Thanks to an immense progress of epitaxial growth techniques, TM oxides heterostructures can now be controlled on atomic length scales. Several novel physical phenomena have been discovered in recent years and potential multifunctional devices seem to be realizable[4–8].

In oxide electronics, one of the cornerstone mechanisms in complex heterostructures (in analogy to semiconductors) is the alignment of bands at a hetero interface and, driven by the resulting potential gradient, a charge transfer across the interface[9–25]. This mechanism can be seen as intrinsic doping without undesired disorder induced by chemical doping. Consequently, controlling heterostructures with a wide variety and range of experimentally tunable parameters (e.g. strain, thickness, substrate choice, etc.) allows to engineer new phases which do not exist in bulk. It is, hence, obvious that predictive power for the direction and amplitude of charge transfer with rules that are as simple as possible is highly desirable.

A natural first attempt would be the usage of well established semiconductor rules, such as Anderson's or the Schottky-Mott rule [26]. As schematically shown in Fig. 1(a) the vacuum energy levels of the two semiconductors on either side of the heterojunction should be aligned, which rely on the electron affinity (or work function) of semiconductors. However, those rules are not suitable for TM oxides, due to the fact that the reduction of the work function to a single value is an approximation that does not hold for TM oxides [27, 28]. Moreover, the characteristic lengthscales in oxides are one or two orders of magnitude smaller than in semiconductors, and hence certain approximations are no longer justified so that non-trivial microscopic terms need to be taken into account explicitly.

In this paper we propose a rule that is based on the continuity of states in the TMO's oxygen matrix and which allows for qualitative prediction of band alignment and charge transfer in complex TMO heterostructures. The oxygen continuity boundary condition allows us to explain and predict the induced charge transfer between the constituents of the heterostructure starting only from energetics of the bulk compounds. In the first part of our report we sketch the underlying driving forces in TMO hetero compounds which are built from perovskites $ABO_3$ with A being the a cation (e.g. Sr or La) and B as a TM from strongly correlated $3d$, $4d$, or strongly spin-orbit coupled $5d$ shell. We claim that bulk data for the oxygen $2p$ energies $\varepsilon_p$ of the components can be used for predictions of $ABO_3/AB'O_3$ interfaces, and prove it by showing quantitative data for a wide range of materials. In the second part of the paper we provide selected examples as a proof of principle, and predictions for possible devices yet to be synthesized.

## II. METHODS

To reveal general material trends, we first study bulk complex transition metal oxides $ABO_3$ with a cubic perovskite structure (in the majority of cases A is taken as Sr but we also discuss other cases like Ca and La) with B being a $3d$ (Ti-Co), $4d$(Zr-Rh) or $5d$ (Hf-Ir) transition metal element. The lattice constant is fixed at the optimized value of $SrTiO_3$, $a$=3.945Å[69]. We then use $SrRuO_3$ as an example for effects of strain, cation A substitution, structural distortion, and magnetism. Most calculations were carried out for superlattices of $(ABO_3)_n/(AB'O_3)_n$ with n=5 and n=1, in order to estimate possible quantum confinement effects for the latter. Moreover, in order to validate the assumption of clean interfaces we performed simulations of a rough interface with a 25% cation mixture (for details see appendix). It turns out that the observed changes are indeed small and will not affect our conclusions. For the study of magnetism in $SrMnO_3$ heterostructures, we take into account an on-site Coulomb interaction $U_{Mn}$=2eV and a realistic $GdFeO_3$-type structural distortion which are considered to be important for a realistic description of the magnetism. In all calculations the atomic positions are fully relaxed.

Density functional theory (DFT) calculations were performed with the VASP (Vienna ab initio simulation package) code [29] using the generalized gradient approximation GGA -PBE functional [30] for electronic exchange and correlation. We consider that energy separation between transition metal $d$ states and oxygen $2p$ states is usually underestimated in the PBE potential, and use the MBJ potential [31], which is implemented in wien2k [32]. We perform Wannier projection [33, 34] of the oxygen $p$ Bloch states and TM $t_{2g}$ $d$ states to obtain an accurate value of the local energy levels $\varepsilon_p$ and $\varepsilon_d$ [35] as shown in Fig. 4 and Table I. Be aware that $\varepsilon_p$ and $\varepsilon_d$ indicate the local energy terms of $t_{2g}$ and oxygen $p$ states respectively and not to the center of gravity for valence or conduction bands ($\varepsilon_v$ and $\varepsilon_c$) [36]. They coincide only in the ionic limit, but for finite covalence (i.e. oxygen-TM hybridization) $\varepsilon_v$ and $\varepsilon_c$ are split apart and the bands have no pure oxygen or TM character anymore. The values in Fig. 4 correspond to $\varepsilon_d$ and $\varepsilon_p$. It turns out that covalence yields an energy drop of approximately 0.4eV of $\varepsilon_p$ for all materials listed in the Fig. 4. We have also carefully checked that the projection details such as including $e_g$ orbitals will not change our conclusion.

In order to obtain quantitative estimates for the charge transfer we integrate the electron density below the Fermi level (down to the energy gap between $d$ and oxygen $p$ states) projected inside atomic spheres. The radius of the atomic spheres (and here is the mentioned ambiguity in the definition) were chosen to the default values of PAW potential in VASP, e.g. 1.2 Angstrom for a Vanadium atom in $SrVO_3$. In this way, the integrated electron density of Vanadium atom in bulk $SrVO_3$ is 0.75. Considering the formal valence of vanadium to be one d electron, we then take 0.75 as renormalizing factor which

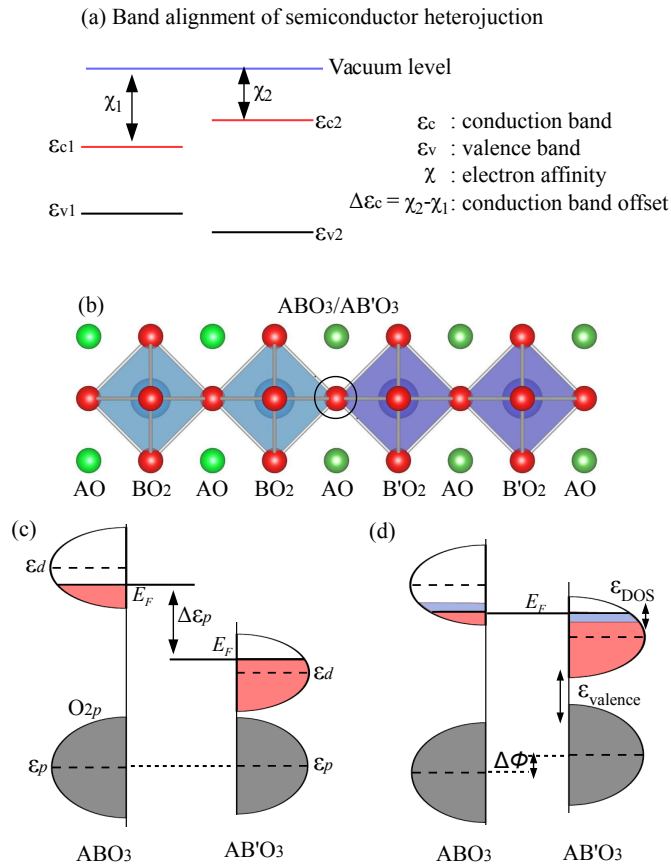


FIG. 1: (a)Schematic figure of Anderson's rule in semiconductor heterojunction: the vacuum energy levels of the two semiconductors on either side are aligned. (b) Schematic figure of a perovskite (001) interface $ABO_3/AB'O_3$ emphasizing the common network of oxygen sites across the interface. (c) Alignment of oxygen states at the interface would generally yield mismatch in the heterostructure's Fermi energy (see Eq. 1). This mismatch drives a charge transfer which itself alters interface and local potentials. The final equilibrium state is shown in (d) with indications (black arrows) of the three different contributions in the energy balance equation Eq. 2. $\varepsilon_p$ and $\varepsilon_d$ are the local energy levels of oxygen $p$ and TM $d$ states.

we also apply to the interface case in order to obtain a quantitative value for the charge transfer. Moreover, in order to estimate the sensitivity of such values with respect to the choice of the radius of atomic spheres, we have checked that a 10% increase of the radius only induces approximately a 3% change of the charge transfer estimated in this way. Hence, the numbers for the charge transfer given in Tab. I have to be taken with some care. We stress that our conclusions do not rely on specific quantitative values, but on overall trends.

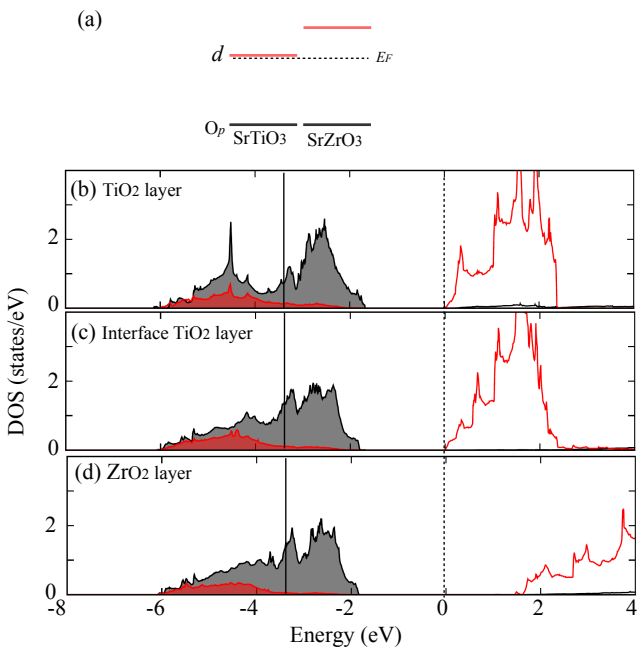


FIG. 2: Sketch of the energy level scheme (a) and layer resolved DFT density of states for the $(SrTiO_3)_5/(SrZrO_3)_5$ superlattice (b,c,d). Oxygen $p$ states (dark gray) and TM $d$ states (red) are shown with the Fermi level marked by the dotted black line. Additionally we show as a solid black line the layer dependent center of mass of the oxygen states which corresponds to the layer dependent $\varepsilon_p^i$. We plot the DOS for the two $BO_2$ layers directly at the interface as well as for the $TiO_2$ two unit cell further away. The alignment of oxygen states in this band insulator heterostructure is practically perfect.

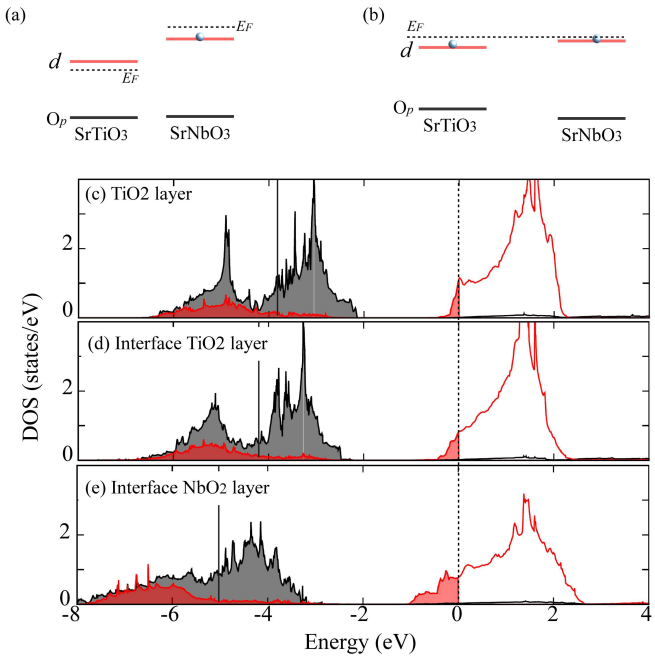


FIG. 3: Upper panel: Sketch of the energy level scheme before (a) and after (b) electron transfer; Lower panels: Same plots as in Fig. 2 now for the heterostructure $(SrTiO_3)_5/(SrNbO_3)_5$. Opposed to the $(SrTiO_3)_5/(SrZrO_3)_5$ we see clear electron transfer across the interface and the expected structure in the alignment of the layer dependent $\varepsilon_p^i$ in the shown layers. The transferred electron into interfacial and bulk TiO2 layers are $0.23e$ and $0.17e$ respectively.

## III. INTRINSIC CHARGE TRANSFER IN COMPLEX OXIDE INTERFACES

Let us start the discussion with the idea that motivated the study. For the sake of simplicity we restrict ourselves to perovskite $ABO_3$ heterostructures along the (001) direction. As common in such TM oxide compounds the most relevant states are i) the empty or partially filled TM $d$ states at the Fermi energy [70] which are split into $t_{2g}$ and $e_g$ states in cubic perovskites and ii) the oxygen $2p$ states residing at an energy $\varepsilon_p$ a few eV below the Fermi energy and forming more or less covalent bonds with the TM $d$ states. At an interface of two materials with different lattice constants or distortion patterns of an ideal cubic case we typically find a smooth transition where such structural features mutually propagate between the components of the heterostructure [37, 38]. A rather natural observation is that such smooth structural transitions in the shared oxygen lattice necessarily demand a continuity of the oxygen states across the interface layers as a boundary condition.

One might start by visualizing the oxygen continuity condition with a very simple sketch we show in Fig. 1(b) for an $ABO_3/AB'O_3$ interface; later on we will extend our discussion to more general cases with different cations. In a hypothetical two step procedure the continuity condition would demand that at the interface the oxygen states need to be lined up which, for two materials with different $\varepsilon_p$, would result in a mismatch of the Fermi energy $E_F$ equivalent to

$$\Delta\varepsilon_p = \varepsilon_p^{\mathrm{ABO_3}} - \varepsilon_p^{\mathrm{AB'O_3}} \tag{1}$$

, see Fig. 1(c). Since $E_F$ must, however, be constant all through the heterostructure in equilibrium, a charge transfer occurs between the layers which itself creates i) an electrostatic potential drop $\Delta\phi$ across the interface, ii) rigid band shifts we indicate by $\Delta\varepsilon_{\mathrm{DOS}}$, and iii) a local electrostatic potential drop $\Delta\varepsilon_{dp}$ yielding relative shifts between TM $d$ and oxygen $p$. These three terms counter the original driving potential - see Fig. 1(d). As indicated in this last sketch we end up with a balance of potentials that has to be calculated self consistently. Before further formalization, let us support this hypothesis by numerical calculations starting with the easiest case of interfacing two band insulators which, in fact, has a one to one correspondence to the band alignment mechanism in semiconductor heterostructures.

In Fig. 2 we show the layer dependent density of states for the interface of $SrTiO_3$ and $SrZrO_3$ simulated in a

5/5 superlattice. The chemical potential, which is basically free to move inside the gap, is indicated by the dashed black line while the center of mass (i.e. the on-site energy) of the oxygen $2p$ states (dark gray DOS) is shown as a black solid line. In the plots, we show $ZrO_2$ and $TiO_2$ layers directly at the interface as well as the $TiO_2$ bulk-like layer two unit cells further away from the interface. As can be seen, the alignment of oxygen states across the interface and even in the next $TiO_2$ layer is practically perfect due to the absence of any charge transfer between the insulating layers. This observation is a first indication of the validity of the backbone hypothesis of the oxygen states continuity. We note in passing that we have an advantage compared to semiconductor heterostructures where obvious structural and electronic continuity is absent[39]. In such semiconducting heterojunctions one might try to employ the Anderson's (or Schottky-Mott) rules in order to estimate the band mismatch by the difference of the components electron affinity (or work function) [26]. It turns out, however, that in realistic cases this rules often fails to predict band offsets. Furthermore, a direct extrapolation of this rule to oxides is rather questionable due to the fact that the concept of a compounds work function is invalid as we have shown in a recent study of oxide heterostructure workfunctions[27, 28] which strongly depend on details of the surface orientation and termination. In contrast, the oxygen state continuity rule is a much stronger boundary condition and, as we point out in several occasions, its predictions seem to agree well with experimental observation.

Now we take one step further and consider $SrNbO_3$ instead of $SrZrO_3$ in the same geometry, i.e. a metal with one valence electron in the Nb $4d$ shell[40], which we show in Fig. 3 - here we see that an initial alignment of oxygen states has lead to electron transfer from Nb $4d$- to Ti $3d$-states across the interface. The self consistently determined final position of oxygen states with respect to the Fermi level is in agreement with the expectations from our sketch in Fig. 1(d). I.e., the transferred electron has lead to an additional potential $\Delta\phi$ in the interface region and changes in the local potentials (discussed in more detail below) which eventually leads to a balanced monotonous evolution of the layer dependent energy of oxygen $2p$ states. Let us stress, that in our picture the directions and relative strength of the charge transfer seem to be predictable just by comparison of $\Delta\varepsilon_p$ of the bulk $ABO_3$.

Before providing numerical data and materials calculations to confirm this, let us give more formal arguments. Indeed, the concept of band alignments at interfaces is well known and understood in semiconducting *pn*-junctions [41], where one observes charge modulations in the so called "space charge" region of the typical order of $\approx$ 100 Å. In the *pn*-junctions two identical semiconductors are interfaced which, however have a Fermi level mismatch due to different, either p- or n-type, kind of doping that is resolved by charge transfer. Yet, in our case there are some crucial differences specific to oxide interfaces: First of all our length-scales are at least one order of magnitude smaller and the variation of the induced potential on the order of a few Å prohibits clearly a semiclassical model commonly used for semiconductors. Secondly, we have to consider more microscopic details for the energy balance equation which finally determines $\Delta n_e$. Namely, in addition to $\Delta\phi$ (the only term of relevance for semiconductor *pn*-junctions) the charge transfer in oxides induces shifts in the local potentials of the different TM sites which might be disentangled into contributions (i) from mutual change of the valence of B and B′ site $\Delta\varepsilon_{dp}$ yielding relative shifts between TM $d$- and oxygen $2p$- states with a sign equal to that of $\Delta n_e$ and ii) from the specific structure of density of states $\Delta\varepsilon_{\mathrm{DOS}}$. In summary we can write

$$-\Delta\varepsilon_p = \Delta\phi + \Delta\varepsilon_{\mathrm{DOS}} + \Delta\varepsilon_{dp} \tag{2}$$

The terms on the right hand side depend on the transferred charge $\Delta n_e$ and we may try to linearize them. For the first term $\Delta\phi$ we can assume a plate capacitor model which would yield a potential drop per unit cell of $\Delta\phi = \Delta n_e \cdot d/\epsilon$ with $d$ being the effective distance of charge transfer cross the interface and $\epsilon$ the dielectric permitivity [42, 43]. The second term can be simplified by assuming an approximately constant density of states around Fermi level $E_F$ to be $\Delta n_e \cdot D$, where $D = \frac{1}{D_B(E_F)} + \frac{1}{D_{B'}(E_F)}$, $D_B$ and $D_{B'}$ the local density of states for B and B′ sites. This contribution D can be seen from Fig. 3 to be of the order of up to 1eV. The last term indicates the change of $\varepsilon_{dp}$ induced by the charge transfer that modifies the valence of transition metal.The argument for the linearity in $\Delta n_e$ of the last term is easily understood by considering a Hartree type self energy ($\propto n_e$) so we can assume $\Delta\varepsilon_{dp} \approx \Delta n_e \cdot U_H$. $U_H$ reflects the change of the energy due to the static single particle mean-field energy that comes from electronic Coulomb interaction. Using virtual crystal approximation for $SrVO_3$ allows us to roughly estimate this contribution to be also of the order of 1eV. Hence, assuming the charge transfer of the order of $\Delta n_e$ =1 will lead, different to semiconductors, to non-negligible contributions of D and $U_H$, since the first term $d/\epsilon$, i.e. the typical length scale, is much smaller in our oxide heterostructures than in semiconductors. We arrive eventually at a simplified linear relation between $\Delta n_e$ and $\varepsilon_p^{\mathrm{bulk}}$:

$$\Delta n_e \approx -\frac{1}{(d/\epsilon + D + U_H)} \cdot \Delta\varepsilon_p \tag{3}$$

While also the simplified equation is hardly solvable in a closed form it allows for a remarkable insight and confirmation of our initial idea: The sign and strength of the charge transfer at an interface between two materials, which turns out to be much larger than in semiconductor devices, should be determined by the difference of the respective bulk oxygen $2p$ energies with respect to their Fermi level $\varepsilon_p$.[71].

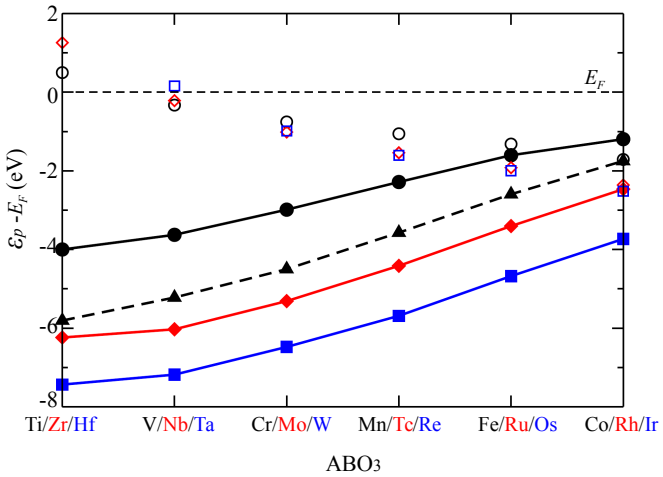


FIG. 4: Summary of bulk $\varepsilon_p$ (filled symbols) and $\varepsilon_d$ (empty symbols) with respect to the Fermi level ($E_F$=0) for different $SrBO_3$ (solid line) materials. For the B site we consider 3$d$ (black), 4$d$ (red), and 5$d$ (blue) elements. With this reference bulk data the charge transfer in heterostructures consisting of these materials can be anticipated. The simple criterion for the direction of the charge transfer at the $ABO_3/AB'O_3$ interface is that the component with lower $\varepsilon_p$ will donate electrons to the other one. Additionally we plot data for $LaBO_3$ (dashed line) for B=3$d$ which is used for estimates for $ABO_3/A'BO_3$ interfaces. (for numerical data of the plot and additional compounds please refer to Tab. III in the appendix)

With this insight we generate DFT reference data for a variety of bulk compounds. The results are summarized in Fig. 4 where we plot the average energy of oxygen 2$p$ states (filled symbols) and the average energy of partially filled d-orbitals (empty symbols) with respect to the Fermi level [72] for $SrBO_3$ (solid lines) with B being a 3$d$ (black), 4$d$ (red), or 5$d$ (blue) element. For the 3$d$ series we additionally show oxygen $p$ energies for $LaBO_3$ (dashed line). The figure nicely shows clear trends in the series of materials considered:

- Within the intra 3$d$, 4$d$, and 5$d$ series we observe a monotonous and almost linear increase of $\varepsilon_p$ of about $2-3$eV within each period.

- Within one group we have a monotonous drop in $\varepsilon_p$ for a given configuration of about $\geq 3$ eV from 3$d$ to 5$d$ compounds.

- Changing Sr to La, i.e. decreasing the oxidation number of the transition metal leads to a decrease of $\varepsilon_p$ up to two eV. This change is actually closely related to $\Delta\varepsilon_{\text{valence}}$ in Eq. 2 and represents in some way the extreme case where we have changed the nominal charge by 1. We note, moreover, that a change of the cation with identical oxidation state ({Sr, Ca, Ba} or { La, Y}) leaves the results for $\varepsilon_p$ basically unchanged, see table Tab. IV in the appendix.

Before we turn to the discussion of how these numbers can be used for predictions we need to address the fact that the results shown in Fig. 4 are all obtained for undistorted cubic unit cells. The energy scale of the listed material trends is of the order of a few eV and it should be emphasized that certain effects beyond idealized structures will lead to modifications of $\varepsilon_p$ on energy scales that are non-negligible compared to our reference data. Therefore we have performed calculations for specific cases studying the influence of strain, orthorhombic distortions, and magnetism (in Tab. IV in the appendix we provide the numerical data for these benchmark cases).

Starting with strain, we see for the example of $SrRuO_3$, that 1% compressive strain will decrease the $\varepsilon_p$ of clearly non-negligible 0.2eV and realize that this effect can actually be additionally exploited to tune the energetics for the desired effect [44, 45]. Next, we turn to orthorhombic distortions [22] in the same material for which we also observe a change of $\varepsilon_p$ of the order of 0.3eV compared to the cubic case which is less but still important for a reliable prediction. Finally, let us address the influence of magnetic order for ferromagnetic $SrRuO_3$. Here we see a split between up and down states not only in the Ru 4d states but also in the associated oxygen states of 0.7eV. We remark that this issue does not occur in antiferromagnetic ordered structures and also for temperatures higher than the Curie temperature. In the FM ordered phase a prediction of the charge transfer by our simplified scheme is not straight forward and becomes questionable if the corresponding energy scales are equal or larger than the $\Delta\varepsilon_p$ in question.

After these remarks, however, we will now show that for many cases the numerical data for the bulk materials shown in Fig. 4 can be exploited in order to predict the charge transfer in layered heterostructures composed of the listed materials. Starting with the compounds shown in Figures 2 and 3, i.e. $SrTiO_3$ interfaces with Sr{Zr, Nb}$O_3$ we start with the bulk values $\varepsilon_p^{SrTiO_3}$=-4.0eV, $\varepsilon_p^{SrZrO_3}$=-6.23eV, and $\varepsilon_p^{SrNbO_3}$=-6.03eV. For the $SrTiO_3/SrZrO_3$ interface both materials show empty TM $d$ states and an alignment of $\varepsilon_p^{SrTiO_3}$ with the lower lying $\varepsilon_p^{SrZrO_3}$ does not result in any electron transfer after equalizing the Fermi levels in line with Eq. 3 due to the diverging $D$ contribution in the right hand side denominator. For the second case, however, we observe that for $SrNbO_3$ the oxygen states are much lower in energy than those of $SrTiO_3$, i.e. $\Delta\varepsilon_p = 2.03\text{eV} \gg 0$. Hence, an alignment of oxygen states would lead to a mismatch of the Fermi energy such that electron needs to be transferred from Nb 4$d$-states to the Ti 3$d$-states for a constant equilibrium chemical potential across the interface. We can exploit the above reported trends in

order to make general predictions:

- Given the monotonous trends within early materials of the same period in the $SrBO_3$ series we conclude that electron transfer will be only possible from lighter to heavier B compounds. This is somewhat counter intuitive: For instance, $d^1$ $SrVO_3$ will transfer its electron to $d^2$ $SrCrO_3$ but not to the empty Ti $3d$ states of $SrTiO_3$. As it turns out, this is in agreement with experiment and other numerical simulations for a variety of interfaces including $LaMnO_3/LaNiO_3$ [17, 46–48], $LaTiO_3/LaFeO_3$ [19, 49, 50], $LaTiO_3/LaNiO_3$ [18, 23], and $SrVO_3/SrMnO_3$ [44, 45].

- Given the monotonous behaviour of $\varepsilon_p$ within one group over different periods we can state that also here electron will be transferred from the heavier to the lighter B element. e.g. $SrNbO_3$ will electron dope $SrVO_3$.

- For the more general case of $ABO_3/AB'O_3$ one has to consider precise values to make predictions. For instance, $SrIrO_3$ should be able to intrinsically dope $SrMnO_3$ at an interface, while $SrRuO_3$ cannot dope $SrTiO_3$.

In order to strengthen the first claim of this list we extend our simulations with a calculation of a $SrTiO_3/SrVO_3$ interface for which we have a $\Delta\varepsilon_p = -0.37$eV. Indeed, consistent with our arguments we see from Fig. 5 that practically no charge transfer occurs. The layer resolved partial density of states shows that basically all $d$ electron remains in the $SrVO_3$ slab and the oxygen $2p$ states are rather well aligned. [73]

At this point it might be asked if our analysis can be applied also to periodic stacks which are further away from the limit of a single interface than the so far considered 5/5 stacks. In order to answer this question we performed several simulations of $(SrBO_3)_1/(SrB'O_3)_1$ heterostructures and summarize the results in Tab. I. Remarkably, we find that in *all* cases the charge transfer can been anticipated in direction and relative amplitude with the data from Fig. 4. This is remarkable since it is not a prior clear that a qualitative argument made for the interface between two bulk materials still holds for a periodic stack with strong quantum confinement effects [51] and lattice relaxations at the interfaces. They are fully taken into account in the heterostructure calculations but do not spoil the predictive capabilities from bulk calculations neither. Looking closer at the values in Tab. I reveals a remarkable consistency between $\Delta\varepsilon_p$ and $\Delta n_e$. We have already seen in the example of the $SrTiO_3/SrVO_3$ interface that in order to dope electron into Ti or V $3d$ states, $4d$ or $5d$ TM components have

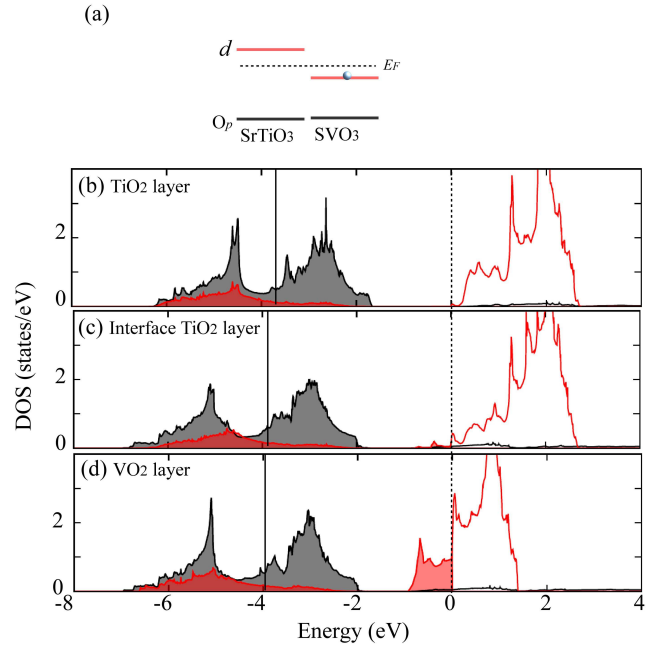


FIG. 5: Same plot as in Figs. 2 and 3 for a $(SrTiO_3)_5/(SrVO_3)_5$heterostructure. In this case alignment of oxygen bands will not drive electron transfer and (as expected from Fig. 4) $SrVO_3$ is a bad candidate for doping $SrTiO_3$

TABLE I: Sign and trends of electron transfer in $(SrBO_3)_1/(SrB'O_3)_1$ heterostructures. We list the energies of oxygen $2p$ states resolved by $BO_2$ ($\varepsilon_p^i(BO_2)$), AO ($\varepsilon_p^i$ (AO)) and $B'O_2$ layers ($\varepsilon_p^i(B'O_2)$) with respect to the Fermi energy as well as the induced electron transfer $\Delta n_e$ from B to B′ sites. $\Delta\varepsilon_p$ taken from Fig. 4 is also listed.

| B/B′ | $\varepsilon_p^i(BO_2)$ | $\varepsilon_p^i(AO)$ | $\varepsilon_p^i(B'O_2)$ | $\Delta n_e$ | $\Delta\varepsilon_p$ |
|---|---|---|---|---|---|
| Ti/Nb | -4.67 | -4.93 | -5.22 | 0.36 | 2.03 |
| Ti/Ta | -5.07 | -5.46 | -5.89 | 0.63 | 3.18 |
| V/Nb | -4.26 | -4.50 | -4.89 | 0.49 | 2.38 |
| V/Ta | -4.62 | -4.92 | - 5.62 | 0.71 | 3.56 |
| V/Cr | -3.72 | -3.61 | -3.60 | -0.27 | -0.64 |
| V/Mn | -3.40 | -3.18 | -3.07 | -0.30 | -1.34 |
| V/Fe | -3.02 | -2.77 | -2.31 | -0.49 | -2.02 |
| V/Co | -2.65 | -2.42 | -1.38 | -0.57 | -2.43 |

to be considered since a positive $\Delta\varepsilon_p$ is needed and, as we can see from the stacks in the first four rows $\Delta n_e$ grows monotonously with $\Delta\varepsilon_p$. The same is true for the opposite case (reported in the lower four rows) where an increased negative $\Delta\varepsilon_p$ drives an increased transfer from the vanadium $3d$ states to heavier elements like Cr, Mn, Fe, and Co in the $3d$ series. Moreover, we can learn from the observation $\Delta\varepsilon_p > \varepsilon_p^i(B) - \varepsilon_p^i(B')$, that for the energy balance (Eq. 2) besides $\Delta\phi$, $\Delta\varepsilon_{DOS}$ and $\Delta\varepsilon_{valence}$ contribute significantly.

Before the end of this section where we have focused mostly on interfaces of the form $SrBO_3/SrB'O_3$

let us make some remarks about the generalization to $ABO_3/A'BO_3$ and the most general $ABO_3/A'B'O_3$ interfaces. In Fig. 4 we have already shown data for $LaBO_3$ in comparison to the $SrBO_3$ series. If we consider the same element on the B site our scheme is directly applicable as before. More specifically, $\varepsilon_p$ of a $LaBO_3$ perovskite is always lower than in the corresponding $SrBO_3$ so that at a $LaBO_3/SrBO_3$ interface the electron is always transferred from $LaBO_3$ to $SrBO_3$ which is consistent with experiments, e.g. for the case of $LaTiO_3/SrTiO_3$ [9, 52] or $LaMnO_3/SrMnO_3$ [13, 16].

Additional complications arise in the most general $ABO_3/A'B'O_3$ setup where we have two qualitatively different interface configurations which might be either AO-$B'O_2$ or $BO_2$-$A'O$. We might actually consider the realistic case of a $SrTiO_3/LaMnO_3$ interface [14, 15, 24, 53]. Starting with the interface $TiO_2$-LaO we assume to have a unit of $LaTiO_3$ linked with $SrTiO_3$ on the one side and $LaMnO_3$ on the other - so we have broken the problem down to a $SrTiO_3/LaTiO_3$ and a $LaTiO_3/LaMnO_3$ interface which we know how to handle. As a result, by considering our reference data, we would arrive at a prediction of charge transfer at the interface from the Ti states of the central $LaTiO_3$ part to its neighbors. The opposite is true for the other possible interface SrO-$MnO_2$, and in this case a decomposition as before would yield the conclusion that no charge transfer will occur. This line of argument is in agreement with experiments on $SrTiO_3/LaMnO_3$ where electron transferred has been observed for the LaO-$TiO_2$ terminated interface [15]. According to our claim, the other interface structure, SrO-$MnO_2$, which experimentally can be realized by inserting a monolayer of $SrMnO_3$, should not allow for such charge transfer. Please note we did not consider the contribution from polar discontinuity [42, 54], which might induce complexity such as oxygen vacancies and other defects.

We conclude our first main section with the claim that charge transfer at the interfaces of perovskite heterostructures can be qualitatively predicted by comparison of bulk qualities. It is not even necessary to perform a numerical simulation of the interface in order to anticipate the direction and relative magnitudes of charge transfer.

## IV. APPLICATIONS AND PREDICTIONS

In the second part of our paper we highlight two applications of our prediction scheme starting with the controlled doping of $SrTiO_3$ (see IV A) drawing also a parallel to heterogeneous semiconductor devices. We then turn to magnetic transitions in manganite heterostructures triggered by controlled charge transfer (see IV B) explaining past theoretical and experimental results in the context of our unifying concept which we then complement by predictions on how to improve external control of such transitions.

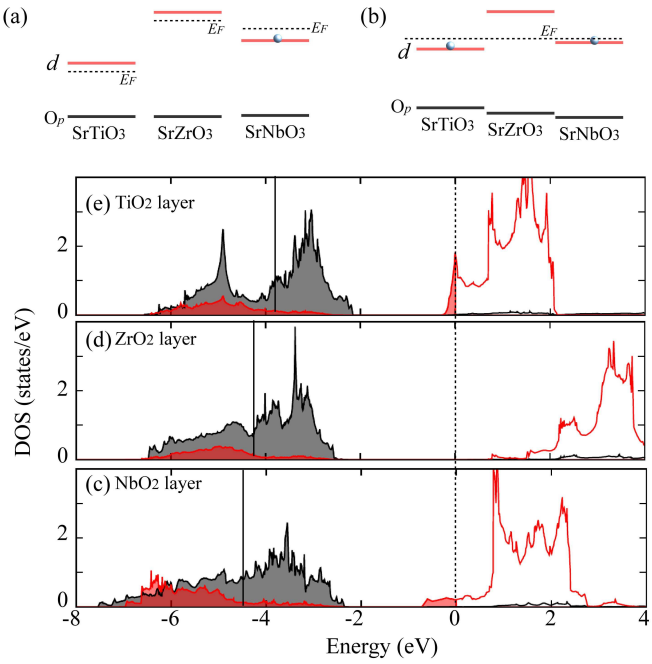


FIG. 6: Same plot as in Fig. 3 but now including an additional buffer layer between $SrTiO_3$ and $SrNbO_3$. The unit cell of this three-component symmetric heterostructure has the form $(SrTiO_3)_5/(SrZrO_3)_2/(SrNbO_3)_1/(SrZrO_3)_2$. As can be seen the electron transfer from Nb to Ti remains intact even after inclusion of the buffer layer excluding a pivotal role of microscopic details in the orbital degrees of freedom at the $SrTiO_3/SrNbO_3$ interface.

### A. Electron doping in $SrTiO_3$ heterostructure

As a first application we chose to highlight how to control doping of one of the most widely spread and used TM oxide compounds $SrTiO_3$. So far $SrTiO_3$ has been doped by various $3d$ TM oxides e.g. $LaAlO_3$ [10] and $LaTiO_3$[9] to produce a two dimensional electron gas but there is no known $SrBO_3$ with B from the $3d$ series. With the data from Fig. 4 we have already given the reason why this is not surprising and, in fact, impossible. The very naive guess that electron from a more filled $3d$ element like, e.g. vanadium would spill into the empty Ti $3d$ states is prohibited by the energy balance that originates in the oxygen states continuity condition (see Fig. 5). So, $SrVO_3$ is identified as a bad candidate for doping $SrTiO_3$. Instead we have seen in Fig. 3 that $SrNbO_3$ is a much more promising component for that purpose. In $(SrTiO_3)_5/(SrNbO_3)_5$ the continuity of oxygen $2p$ states drives a sizable charge transfer. What we have not discussed yet, however, is the question if microscopic details of orbital degrees of freedom at the interface, which are not included in our scheme, are equally or even more important for the charge transfer than the considered energetics. In order to shed light on this issue we extend our calculations with the inclusion of an insulating buffer

layer which will allow for a spatial separation of Ti and Nb $d$-states. The choice of a perovskite buffer layer is actually quite straight forward in the light of our reference data and we chose $SrZrO_3$ for this purpose which will remain band insulating in the three component heterostructure. In Fig. 5 we show the result for a symmetric $(SrTiO_3)_5/(SrZrO_3)_2/(SrNbO_3)_1/(SrZrO_3)_2$ superlattice which is experimentally realizable[21, 55–57].

Here we see another confirmation of our simple argument: while the buffer layer remains band insulating we still observe a transfer of electron from Nb to Ti $d$-states even though they are spatially separated. At this point we might refer to an analogous technique in semiconductor setups where the doping impurities are spatially separated from the charge carriers. A concept which is commonly known as "modulation doping" and widely applied in so called MODFET setups [58, 59]. Besides the shown results we have checked the dependence of the charge transfer amplitude as a function of the thickness of the buffer layer but were unable to find significant trends up to supercells that include buffers of 5 bulk unit cells. In fact modulation doped oxides recently started to attract some theoretical [43] and experimental [21, 53, 57] researchers.

### B. AFM to FM transition in $SrMnO_3$ heterostructures

After having exemplified how our oxygen energetics argument can be used to anticipate charge transfer in the case of $SrTiO_3$ based heterostructures we now take one step further by considering manganite heterostructures. Here the goal is similar yet more ambitious since a provoked charge transfer in $SrMnO_3$ setups should have a sensitive impact on magnetic transitions. Starting point for us is bulk $SrMnO_3$ which is found to have a G-type antiferromagnetic ground state. Our goal is to find an appropriate heterostructure in which doping into Mn $d$-states triggers a transition to a ferromagnetic ground state - see review papers [60–63] and references therein. From our reference data we see that it should actually be rather easy to provoke electron transfer into Mn $d$-states considering the comparatively large value of $\varepsilon_p$ for Mn. Indeed it turns out that by employing our predictive scheme we can confirm experimentally known routes to charge-transfer induced magnetic transition and classify possible heterostructure components to tune more or less charge transfer.

We carried out calculations for 1/1 and 2/2 layered superlattice $(SrMnO_3)_1/(SrBO_3)_1$ (considering also a $GdFeO_3$ structural distortion since magnetism can be strongly coupled to the lattice) for four different species of B site elements. The results are summarized in Tab. II where we report the size of the magnetic moment on the B and the Mn site of the respective compound. We have sorted the table with ascending electron transfer. As anticipated choosing $SrIrO_3$ as interfacing partner will result in a little electron transfer and, in the 2/2 structure the antiferromagnetic order with a moment of 3.05 $\mu_B$ remains. In the case of the 1/1 structure we observe a somewhat larger electron transfer which is already sufficient to trigger a magnetic transition to a ferromagnetic ground state [25] with ordered Mn moments of 3.24 $\mu_B$. The next component we consider is $SrVO_3$ - here the data from Fig. 2 tells us to expect similar to the Ir compound only a small amount of transferred electron which we see confirmed in our numerical results. Interestingly, both 1/1 and 2/2 compounds seem to be intermediate between antiferromagnetic and ferromagnetic phase yielding a ferrimagnetic ground state[44, 45]. We can further predict which components would yield a much more significant electron transfer: Candidates are easily nominated from Fig. 4 and to this end we select $SrNbO_3$, which is recently grown experimentally[40], as well as $SrTaO_3$ - our most potent electron donor for oxide heterostructures. The selected components perform as predicted in the numerical simulations and we observe a large charge transfer pushing the $(SrMnO_3)_{1,2}/(SrNbO_3)_{1,2}$ and $(SrMnO_3)_{1,2}/(SrTaO_3)_{1,2}$ into a ferromagnetic metallic ground state with ordered Mn moments up to $3.74\mu_B$.[74]

TABLE II: Magnetic ground states of $(SrBO_3)_n/(SrMnO_3)_n$ with $n$=1,2. B = Ir, V, Nb, and Ta. The magnetic moments localized on TM B and Mn sites are also listed.

| | 1/1 | | | 2/2 | | |
|---|---|---|---|---|---|---|
| | B ($\mu_B$) | Mn($\mu_B$) | M | B($\mu_B$) | Mn($\mu_B$) | M |
| $SrIrO_3$ | 0.0 | 3.24 | Ferro | 0.0 | 3.05 | AFM |
| $SrVO_3$ | -0.19 | 3.2 | Ferri | -0.36 | 3.16 | Ferri |
| $SrNbO_3$ | 0.05 | 3.66 | Ferro | 0.02 | 3.56 | Ferro |
| $SrTaO_3$ | 0.03 | 3.74 | Ferro | 0.0 | 3.67 | Ferro |

In order to underline the data given in Tab. II we plot the resolved single particle density of states in Fig. 7 - this time, however, for magnetic DFT calculations. In the upper panels of the figure we start as a reference with the bulk results for the gapped antiferromagnetic DOS of $SrMnO_3$ and metallic and paramagnetic $SrTaO_3$. In the lower two panels one can nicely observe how in the $(SrMnO_3)_1/(SrTaO_3)_1$ heterostructure almost all Ta $d$ electron is depleted in the $MnO_2$ layers yielding a metallic ferromagnetic ground state with significant filling of the Mn $3d$-$e_g$ states.

## V. SUMMARY AND OUTLOOK

In summary we have presented a simple prediction scheme for the tuning of charge transfer in oxide heterostructures. By employing arguments based on the requirement that the $p$ states of the oxygen network in a heterostructure need to be continuous, we were able to utilize reference data from bulk calculations in Fig. 4 to predict the direction and relative amplitude of charge

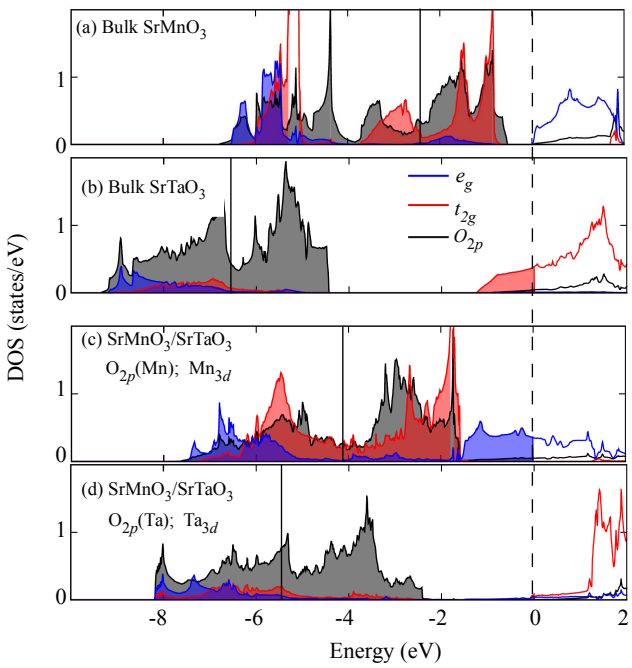


FIG. 7: Plot of the density of states with the usual color/marker convention (including now also $3d$-$e_g$ states plotted in blue). We show results for magnetically ordered calculations starting with bulk results in the upper two panels. $SrMnO_3$ is G-type antiferromagnetic ordered and $SrTaO_3$ paramagnetic. In the lower two panels we plot the data for the two layers in a $(SrMnO_3)_1/(SrTaO_3)_1$ heterostructure including a $GdFeO_3$ distortion. We see the dramatic influence of the electron transfer from Ta to Mn and the induction of ferromagnetic ordered metallic $MnO_2$ layers.

transfer between layers in oxide heterostructures. Remarkably this scheme remains in tact even for layered compounds down to a 1/1 geometry. As a proof of principle we provided simulations for electron doping of $SrTiO_3$ in heterogeneous arrays simultaneously confirming experimentally known trends and offering suggestions to material growers which are the most promising components to control the low energy electronic structure. In a second application part we have exemplified, with the help of $SrMnO_3$ based heterostructures, how controlled charge transfer can be systematically exploited in order to trigger magnetic phase transitions. The shown examples are only a taste of what can be predicted with the unifying concepts we presented and we hope that experimental colleagues will be inspired by our work to create new materials and devices. This includes specifically also the possibility to couple/entangle - via charge transfer - physics of $3d$ and $5d$ TM oxides [25, 64] which, each on their own, are governed by very different energy scales. One might try, for instance, to induce spin-orbit coupling effects in $3d$ systems, e.g. in the case of $SrMnO_3$ /$SrTaO_3$ where one might find a large magnetic anisotropy energy and antisymmetric exchange on the magnetic Mn sites. One might even target the realization of yet more exotic skyrmion, spin-spiral, and topological phases. On the computational side we already started a hunt for the best possible candidates to be manipulated towards exciting new ground states.

In order to give an outlook for future theory and computational development we state once more that for certain cases the application of our scheme is not straight forward and needs to be extended. One of these cases is the interfacing of compounds that are ferromagnetic ordered in bulk. Another issue that should be mentioned is the change of $\varepsilon_p$ due to correlation effects: Given that the relevant effects we discussed have a characteristic energy scale of a few eV, shifts due to single particle self energies might have to be included instead of the simplified $\Delta\varepsilon_{dp}$ contribution in Eq. 2. A very clear example where this will be the case is the usage of charge transfer insulators, typically found in late $3d$ TM oxides e.g. cuprates. An extension to include such correlation effects is very desirable since the sensitivity of correlated electron systems would add even more possibilities to generate novel functionality like, e.g. the recently suggested Mott transistor[65]. Moreover, focusing more on material trends the presented initial study did not extensively discuss how to use the thickness of periodic stacks or buffer layers to quantitatively tune charge transfer and how to interface non-perovskite oxides. The oxygen continuity condition, or adaptations thereof, should be valid not only in the complex oxides with perovskite structures, but also in other lattice structures like anatase, pyrochlores, spinel, Ruddlesden-Popper and double perovskites [66–68] which are structurally equal to the 1/1 interfaces along a (111) direction.

## VI. ACKNOWLEDGMENTS

We thank H. Boschker, J. Nichols, H. N. Lee, Y. Lu, L. Si, Z. Liao, Z. Wang, Y. Cao and J. Mannhart for motivation and valuable discussions.

### Appendix A: Simulation of a rough surface

To test the effect of cation mixing we have performed benchmark calculations with up to 25% mixing. To this end we employ a 2×2 supercell with a layered structure as -$BO_2$-AO-$B_{0.75}B'_{0.25}O_2$-AO-$B_{0.25}B'_{0.75}O_2$-AO-$B'O_2$. The comparison between the density of states for clean and rough interfaces with (and without) charge transfer is shown in Fig.8. Our main conclusion remains, hence, unchanged, and effects like cation mixing can indeed be regarded as a secondary effect.

### Appendix B: Numerical data

In Tab. III we provide the numerical data plotted in Fig. 4. Moreover, in Tab. IV we report values of $\varepsilon_p$

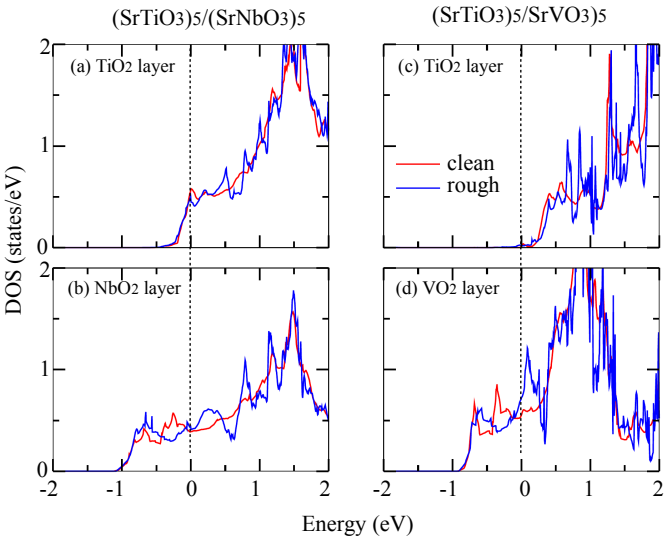


FIG. 8: Projected Density of TM $t_{2g}$ states of the $BO_2$ layer with two layers away from interface. Red indicates a clean interface, while blue indicates a rough interface with 25% cation intermixing.

for benchmark calculations including effects of cation exchange, orthorhombic distortion, strain, and ferromagnetic ordering.


[1] H. Kroemer, Rev. Mod. Phys. **73**, 783 (2001).
[2] M. Imada, A. Fujimori, and Y. Tokura, Rev. Mod. Phys. **70**, 1039 (1998).
[3] Y. Tokura and N. Nagaosa, Science **288**, 462 (2000).
[4] J. Mannhart and D. G. Schlom, Science **327**, 1607 (2010).
[5] H. Takagi and H. Y. Hwang, Science **327**, 1601 (2010).
[6] P. Zubko, S. Gariglio, M. Gabay, P. Ghosez, and J.-M. Triscone, Annual Review of Condensed Matter Physics **2**, 141 (2011).
[7] H. Y. Hwang, Y. Iwasa, M. Kawasaki, B. Keimer, N. Nagaosa, and Y. Tokura, Nat. Mat. **11**, 103 (2012).
[8] J. Chakhalian, A. J. Millis, and J. Rondinel, Nat. Mat. **11**, 92 (2012).
[9] A. Ohtomo, D. A. Muller, J. L. Grazul, and H. Y. Hwang, Nature **419**, 378 (2002).
[10] A. Ohtomo and H. Y. Hwang, Nature **427**, 423 (2004).
[11] I. Gonzlez, S. Okamoto, S. Yunoki, A. Moreo, and E. Dagotto, Journal of Physics: Condensed Matter **20**, 264002 (2008).
[12] G. Logvenov, A. Gozar, and I. Bozovic, Science **326**, 699 (2009).
[13] S. J. May, P. J. Ryan, J. L. Robertson, J.-W. Kim, T. S. Santos, E. Karapetrova, J. L. Zarestky, X. Zhai, S. G. E. te Velthuis, J. N. Eckstein, et al., Nat. Mat. **8**, 892 (2009).
[14] J. Garcia-Barriocanal, J. Cezar, F. Bruno, P. Thakur, N. Brookes, C. Utfeld, A. Rivera-Calzada, S. Giblin, J. Taylor, J. Duffy, et al., Nat. Comm. **10**, 1038 (2010).
[15] J. Garcia-Barriocanal, F. Y. Bruno, A. Rivera-Calzada, Z. Sefrioui, N. M. Nemes, M. Garcia-Hernndez, J. Rubio-Zuazo, G. R. Castro, M. Varela, S. J. Pennycook, et al., Advanced Materials **22**, 627 (2010).
[16] A. Bhattacharya, S. J. May, S. G. E. te Velthuis, M. Warusawithana, X. Zhai, B. Jiang, J.-M. Zuo, M. R. Fitzsimmons, S. D. Bader, and J. N. Eckstein, Phys. Rev. Lett. **100**, 257203 (2008).
[17] M. Gibert, P. Zubko, R. Scherwitzl, J. Iniguez, and J.-M. Triscone, Nat. Mat. **11**, 195 (2009).
[18] H. Chen, A. J. Millis, and C. A. Marianetti, Phys. Rev. Lett. **111**, 116403 (2013).
[19] J. E. Kleibeuker, Z. Zhong, H. Nishikawa, J. Gabel, A. Müller, F. Pfaff, M. Sing, K. Held, R. Claessen, G. Koster, et al., Phys. Rev. Lett. **113**, 237402 (2014).
[20] J. Salafranca, J. Rincón, J. Tornos, C. León, J. Santamaria, E. Dagotto, S. J. Pennycook, and M. Varela, Phys. Rev. Lett. **112**, 196802 (2014).
[21] Y. Chen, F. Trier, T. Kasama, D. V. Christensen, N. Bovet, Z. I. Balogh, H. Li, K. T. S. Thydn, W. Zhang, S. Yazdi, et al., Nano Letters **15**, 1849 (2015).
[22] M. N. Grisolia, J. Varignon, G. Sanchez-Santolino, A. Arora, S. Valencia, M. Varela, R. Abrudan, E. Weschke, E. Schierle, J. E. Rault, et al., Nat. Phys. **12**, 484 (2016).
[23] Y. Cao, X. Liu, M. Kareev, D. Choudhury, S. Middey, D. Meyers, J.-W. Kim, P. Ryan, J. Freeland, and J. Chakhalian, Nat. Comm. **7**, 10418 (2016).
[24] X. R. Wang, C. J. Li, W. M. Lü, T. R. Paudel, D. P. Leusink, M. Hoek, N. Poccia, A. Vailionis, T. Venkatesan, J. M. D. Coey, et al., Science **349**, 716 (2015).
[25] J. Nichols, X. Gao, S. Lee, T. L. Meyer, J. W. Freeland, V. Lauter, D. Yi, J. Liu, D. Haskel, J. R. Petrie, et al., Nat. Comm. **7**, 12721 (2016).
[26] J. H. Davies, The Physics of Low-Dimensional Semiconductors, Cambridge University Press (1997).
[27] Z. Zhong and P. Hansmann, Phys. Rev. B **93**, 235116

(2016).
[28] R. Jacobs, J. Booske, and D. Morgan, Advanced Functional Materials **26**, 5471 (2016).
[29] G. Kresse and D. Joubert, Phys. Rev. B **59**, 1758 (1999).
[30] J. P. Perdew, K. Burke, and M. Ernzerhof, Phys. Rev. Lett. **77**, 3865 (1996).
[31] F. Tran and P. Blaha, Phys. Rev. Lett. **102**, 226401 (2009).
[32] P. Blaha, K. Schwarz, G. K. H. Madsen, D. Kvasnicka, and J. Luitz, *WIEN2k, An Augmented Plane Wave + Local Orbitals Program for Calculating Crystal Properties* (Karlheinz Schwarz, Techn. Universität Wien, Austria, 2001), ISBN 3-9501031-1-2.
[33] J. Kune, R. Arita, P. Wissgott, A. Toschi, H. Ikeda, and K. Held, Computer Physics Communications **181**, 1888 (2010).
[34] A. A. Mostofi, J. R. Yates, Y.-S. Lee, I. Souza, D. Vanderbilt, and N. Marzari, Computer Physics Communications **178**, 685 (2008).
[35] M. W. Haverkort, M. Zwierzycki, and O. K. Andersen, Phys. Rev. B **85**, 165113 (2012).
[36] C. Noguera, Physics and chemistry at oxide surfaces, Cambridge University Press (1996).
[37] J. M. Rondinelli and N. A. Spaldin, Advanced Materials **23**, 3363 (2011).
[38] Z. Liao, M. Huijben, Z. Zhong, N. Gauquelin, S. Macke, R. J. Green, S. V. Aert, J. Verbeeck, G. V. Tendeloo, K. Held, et al., Nat. Mat. **15**, 425 (2016).
[39] J. Tersoff, Phys. Rev. B **30**, 4874 (1984).
[40] D. Oka, Y. Hirose, S. Nakao, T. Fukumura, and T. Hasegawa, Phys. Rev. B **92**, 205102 (2015).
[41] N. W. Ashcroft and N. D. Mermin, Solid State Physics, Holt, Rinehart and Winston (Philadelphia, 1976).
[42] N. Nakagawa, H. Y. Hwang, and D. A. Muller, Nature Materials **5**, 204 (2006).
[43] Z. Zhong, P. X. Xu, and P. J. Kelly, Phys. Rev. B **82**, 165127 (2010).
[44] H. Chen, H. Park, A. J. Millis, and C. A. Marianetti, Phys. Rev. B **90**, 245138 (2014).
[45] A. Tseng, A. Pham, S. C. Smith, and S. Li, Journal of Applied Physics **119**, 075301 (2016).
[46] S. Dong and E. Dagotto, Phys. Rev. B **87**, 195116 (2013).
[47] A. T. Lee and M. J. Han, Phys. Rev. B **88**, 035126 (2013).
[48] J. Hoffman, I. C. Tung, B. B. Nelson-Cheeseman, M. Liu, J. W. Freeland, and A. Bhattacharya, Phys. Rev. B **88**, 144411 (2013).
[49] H. Zhang, Y. Weng, X. Yao, and S. Dong, Phys. Rev. B **91**, 195145 (2015).
[50] X. He and K.-j. Jin, Phys. Rev. B **93**, 161108 (2016).
[51] Z. Zhong, Q. Zhang, and K. Held, Phys. Rev. B **88**, 125401 (2013).
[52] S. Okamoto and A. J. Millis, Nature **428**, 630 (2004).
[53] Y. Z. Chen, F. Trier, T. Wijnands, R. J. Green, N. Gauquelin, R. Egoavil, D. V. Christensen, G. Koster, M. Huijben, N. Bovet, et al., Nat. Mat. **14**, 801 (2015).
[54] C. Noguera, Journal of Physics: Condensed Matter **12**, R367 (2000), URL `http://stacks.iop.org/0953-8984/12/i=31/a=201`.
[55] A. Beck, J. G. Bednorz, C. Gerber, C. Rossel, and D. Widmer, Applied Physics Letters **77** (2000).
[56] M. Moreira, J. Andrs, V. Longo, M. Li, J. Varela, and E. Longo, Chemical Physics Letters **473**, 293 (2009).
[57] A. P. Kajdos, D. G. Ouellette, T. A. Cain, and S. Stemmer, Applied Physics Letters **103**, 082120 (2013).
[58] R. Dingle, H. L. Strmer, A. C. Gossard, and W. Wiegmann, Applied Physics Letters **33** (1978).
[59] T. Mimura, S. Hiyamizu, T. Fujii, and K. Nanbu, Japanese Journal of Applied Physics **19**, L225 (1980).
[60] J. M. D. Coey, M. Viret, and S. von Molnr, Advances in Physics **48**, 167 (1999).
[61] E. Dagotto, T. Hotta, and A. Moreo, Physics Reports **344**, 1 (2001).
[62] M. B. Salamon and M. Jaime, Rev. Mod. Phys. **73**, 583 (2001).
[63] Y. Tokura, Reports on Progress in Physics **69**, 797 (2006).
[64] W.-G. Yin, X. Liu, A. M. Tsvelik, M. P. M. Dean, M. H. Upton, J. Kim, D. Casa, A. Said, T. Gog, T. F. Qi, et al., Phys. Rev. Lett. **111**, 057202 (2013).
[65] Z. Zhong, M. Wallerberger, J. M. Tomczak, C. Taranto, N. Parragh, A. Toschi, G. Sangiovanni, and K. Held, Phys. Rev. Lett. **114**, 246401 (2015).
[66] Y. Tomioka, T. Okuda, Y. Okimoto, R. Kumai, K.-I. Kobayashi, and Y. Tokura, Phys. Rev. B **61**, 422 (2000).
[67] K. Kato, Y. Moritomo, M. Takata, M. Sakata, M. Umekawa, N. Hamada, S. Ohkoshi, H. Tokoro, and K. Hashimoto, Phys. Rev. Lett. **91**, 255502 (2003).
[68] Y. W. Long, N. Hayashi, T. Saito, M. Azuma, S. Muranaka, and Y. Shimakawa, Nature **458**, 60 (2009).
[69] The DFT-GGA optimized lattice constant for $SrTiO_3$ is $a$=3.945Å, which is about 1% larger than the experimental one. Our estimates of effects from strain show that such effects are negligible for the conclusions we draw.
[70] In band insulating materials such as $SrTiO_3$, it turns out (from several DFT simulations of the material) that the assumption of a slight $n$-type doping ($E_F$ at the bottom of the conduction band) is the appropriate choice.
[71] Let us, finally, remark that this relation also holds for the case of band insulating interfaces (i.e. vanishing density of states at $E_F$) where D will diverge and, hence an infinitesimal $\Delta n_e$ leads to finite $\Delta\varepsilon_p$
[72] The change of $E_F$ within the series is quite small, e.g $E_F(SrVO_3)$=5.20eV, $E_F(SrMnO_3)$=5.13eV
[73] At a closer look one should note a very small amount of charge at the interface $TiO_2$ (concomitant with a non-perfect oxygen alignment) layer which one might attribute to a covalent hybridization of Ti and V d-states directly at the interface. However, as we will see in the next step, this effect is very small compared to the charge transfer one can obtain by replacing $SrVO_3$ with another compound.
[74] Let us remark once more that, due to additional confinement effects, the 1/1 compounds are the materials "furthest away" from a single interface situation so that some exceptions to the trends are quite expected - it is actually rather remarkable how well most of the predictions from bulk energetics still work!

TABLE III: Numerical data of Fig. 4 $\varepsilon_p$ of $SrBO_3$ with B=3$d$, 4$d$, and 5$d$. The unit is eV

| 3$d$ | $\varepsilon_p$ | 4$d$ | $\varepsilon_p$ | 5$d$ | $\varepsilon_p$ |
|---|---|---|---|---|---|
| $SrTiO_3$ | -4.00 | $SrZrO_3$ | -6.23 | $SrHfO_3$ | -7.43 |
| $SrVO_3$ | -3.63 | $SrNbO_3$ | -6.03 | $SrTaO_3$ | -7.18 |
| $SrCrO_3$ | -2.99 | $SrMoO_3$ | -5.31 | $SrWO_3$ | -6.48 |
| $SrMnO_3$ | -2.28 | $SrTcO_3$ | -4.41 | $SrReO_3$ | -5.69 |
| $SrFeO_3$ | -1.60 | $SrRuO_3$ | -3.40 | $SrOsO_3$ | -4.68 |
| $SrCoO_3$ | -1.19 | $SrRhO_3$ | -2.47 | $SrIrO_3$ | -3.73 |

TABLE IV: Reference data for $\varepsilon_p$ of manganites and ruthenates depending on cation exchange, othorhombic distortion, compressive strain and ferromagnetic ordering. The unit is eV

| Manganites | $\varepsilon_p$ | Ruthenates | $\varepsilon_p$ |
|---|---|---|---|
| $KMnO_3$ | -1.47 | $KRuO_3$ | -2.48 |
| $CaMnO_3$ | -2.30 | $CaRuO_3$ | -3.44 |
| $BaMnO_3$ | -2.22 | $BaRuO_3$ | -3.29 |
| $LaMnO_3$ | -3.57 | $LaRuO_3$ | -4.56 |
| $SrMnO_3$ | -2.28 | $SrRuO_3$ | -3.40 |
| 1% compressive $SrMnO_3$ | -2.42 | $SrRuO_3$ | -3.60 |
| distorted $CaMnO_3$ | -2.70 | $SrRuO_3$ | -3.72 |
| FM $SrMnO_3$ | -2.25/-2.75 | $SrRuO_3$ | -3.46/-4.17 |